^{139}La NMR in lanthanum manganites: Indication of the presence of magnetic polarons from spectra and nuclear relaxations

G. Allodi, R. De Renzi, and G. Guidi
Dipartimento di Fisica e Istituto Nazionale di Fisica della Materia, Università di Parma, 43100 Parma, Italy
(Received 3 July 1997; revised manuscript received 2 September 1997)

We present ^{139}La NMR experiments on five powder samples of lanthanum manganites, with a Mn^{4+} concentration ranging from the antiferromagnetic-insulator (AFM) to the ferromagnetic-conducting (FM) region of the phase diagram. We measure a positive hyperfine coupling $\mathcal{C}=0.13$ T/μ_B. A signal from nuclei in a FM environment is present at all compositions, as evidenced by a hyperfine frequency in zero-field experiments, by a positive hyperfine shift in NMR experiments below T_c, and by a paramagnetic frequency shift following Curie-Weiss law. A signal from nuclei in an AFM environment is identified by a similar negative intercept Curie-Weiss law. The NMR spectra reveal a large temperature dependent fraction of static spin defects below T_c in the FM domains. Nuclear relaxation indicates that the FM regions are influenced by diffusing, AFM-correlated excitations, while the AFM regions probe spin fluctuations from diffusing, FM correlated excitations. These results are interpreted in terms of electronic inhomogeneities due to the presence of a magnetic small polaron. [S0163-1829(98)04602-5]

I. INTRODUCTION

Lanthanum manganites were first studied in the 1950's for their peculiar phase diagram where antiferromagnetism (AFM) is associated with insulating properties and ferromagnetism (FM) with metallicity.[1] Their magnetic and transport properties are controlled by the Mn^{3+}-Mn^{4+} ratio, which in turns is determined by either cation vacancies or heterovalent cation substitution. In recent years these materials have attracted renewed interest, after the discovery of *colossal* magnetoresistive effects; lanthanum manganites doped with alkali-earth metals were discovered to exhibit a negative magnetoresistance[2–4] of up to 10 000% (in thin films of $La_{1-y}Ca_yMnO_3$ at 77 K and 9.1 T) around the Curie temperature. Most of the recent experimental work is addressed to the transport and magnetic properties of the fully FM compounds, where the peak in the magnetoresistance is closest to room temperature (therefore more promising for applications).

FM order is qualitatively justified by double exchange (DE), where the formation of a ferromagnetic band in the presence of a strong interaction with Hund rule localized moments reduces the total energy of the system.[5] On this basis early descriptions[6,7] and mean-field models[8,9] predict a metallic FM phase around an optimum doping, $x=0.3$, and a transition to an AFM insulator at lower doping. This simplified phase diagram (DE only) roughly agrees with neutron results.[10] In particular, neutron data reveal coexisting AFM and FM diffraction peaks around $x=0.15$, which have been interpreted in terms of an intermediate homogeneous canted arrangement of spins.[8,11]

However, several authors have recently argued[12–14] that the colossal magnetoresistive behavior cannot appear without the inclusion of a strong electron-phonon coupling, leading to the formation of Jahn-Teller (JT) polarons. In this scenario, charge carriers bring along an induced lattice distortion, which originates from the degeneracy of the electronic ground state rather than from direct polarization effects.

Direct evidence of the polaron presence was provided by the close agreement between a superparamagnetic anomaly in the magnetization and an enhanced small angle neutron scattering around the magnetic ordering transition.[15] Further evidence of polaron formation and of its relevance to the magnetic properties of the manganites was provided by giant isotope shifts of the Curie temperature.[16,17] JT polarons drastically modify the interpretation of the phase diagram: on one hand, the observed Curie temperatures are proportional to the effective bandwidth of the polaron[18,16] (hence the isotope effect); on the other hand, their presence may give rise to electronically driven inhomogeneities,[19] akin to the electronic phase separation discussed in the context of high-T_c superconductors. ^{55}Mn NMR data[20] showed that at liquid helium temperature phase separation into FM and AFM microdomains does occur throughout the entire $0\leqslant x<0.25$ range, whereas the canting of the DE-only phase diagram was never detected. Moreover, direct evidence of magnetic correlations between the two types of micro-domains was provided by the nuclear longitudinal relaxation functions.

Unfortunately, ^{55}Mn NMR is not suitable for an investigation at higher temperature, since the signal is lost very soon because of fast transverse relaxations. The La nucleus is coupled to the eight surrounding Mn ions by transferred hyperfine interactions, and thus it is a local probe of the Mn magnetization. La NMR signals from magnetically ordered $LaMnO_3$ have already been reported.[21] In this work the same samples of Ref. 20 are investigated by ^{139}La NMR in a wider temperature interval across the transitions. We provide further evidence from spectra and relaxations of a microscopically inhomogeneous structure and dynamics, which we propose to interpret in terms of localized small polarons.

The paper is organized in three main sections. Section II describes briefly the sample preparation and characterization, as well as the basic NMR measurements. The results are

TABLE I. Transition temperatures from susceptibility measurements at 44 MHz (Ref. 25).

	va.00	va.11	Ca.20	va.16	Ca.23
T_c (K)	115(1)	106(1)	180(1)	237(1)	262(1)

given in Sec. III in the following order: zero- and low-field spectra in nominally FM samples (Sec. III A), high-field spectra in FM samples (Sec. III B), high-field spectra on nominally AFM va.00 (Sec. III C) and finally relaxation rate measurements (Sec. III D). All our findings are discussed in Sec. IV evidencing the intrinsic inhomogeneous nature of these materials.

II. EXPERIMENTAL DETAILS

A. Samples and apparatus

We performed ^{139}La NMR spin echo experiments on five samples of powdered lanthanum manganites in the range $0<x<0.25$: three are hole doped by stoichiometric defects, and two by the Ca-La substitution. The unsubstituted compounds, $(LaMn)_{1-x/6}O_3$, were annealed in vacuum. In these conditions it is the amount of cation vacancies,[22] determined by annealing temperatures in the range $1200<T_a<1350$ °C, which controls the mean valence of Mn, $3+x$. The mean valence was measured by titration in the three unsubstituted samples,[23] yielding nominal fractions of Mn^{4+}, respectively, $x=0.0$, 0.11, and 0.16. We shall refer to these samples as va.00, va.11, and va.16.

The two $La_{1-y}Ca_yMnO_3$ samples were both annealed at 1300 °C, and their nominal fraction of of Mn^{4+} ions was measured by titration to be $x=0.20\pm0.02$ and $x=0.23\pm0.02$. In the following they are referred to as Ca.20 and Ca.23, respectively.

X-ray diffraction spectra revealed a single phase in all five samples, with lattice parameters and symmetry class in accordance with literature data.[10,24]

Referring to the DE-only phase diagram, va.00 and va.11 belong to the AFM-insulating region, while Ca.20, Ca.23, and va.16 belong to the FM-metallic region. However, ferromagnetic transitions were detected by radio frequency susceptibility measurements[25] in all samples. Ca.20, Ca.23, and va.16 display large low temperature contributions to $\chi_{\rm rf}$ from a nonlinear FM magnetization and a sharp drop at the transition. In contrast, samples va.00 and va.11 show a peak at the transition and a very much smaller contribution below [this reflects the fact that for the former $\max(\chi)>1/N$, while for the latter $\max(\chi)\ll 1/N$, where $N\approx 1/3$ is the average grain demagnetization factor). All observed transition temperatures are listed in Table I.

The fact that sample Ca.20 displays a lower T_c than sample va.16 agrees with the trend of the Mn NMR findings,[20] and is understood as a cation size effect.[26]

In the following we shall often consider together the two samples va.00 and va.11, which show almost no sign of macroscopic magnetization, and the three samples va.16, Ca.20, and Ca.23, which display large macroscopic magnetic moments. For the sake of simplicity we shall loosely refer to the first group as *antiferromagnetic* (AFM) *samples* and to the second as *ferromagnetic* (FM) *samples*, despite the presence of a ferromagnetic response in all of them.

The ^{139}La spin-echo NMR experiments were performed in the temperature range 20–360 K on a Stelar spectrometer. We studied the resonances in zero magnetic field, in an electromagnet up to 1.2 T and in a 7 T superconducting solenoid. The rf pulse train was fed to a gated class A linear amplifier. The spectra were taken by varying the transmitter frequency and recording point by point the peak Fourier amplitude of the echo signal. Transverse relaxations were measured by varying the delay τ in the spin echo sequence, according to the scheme ϕ-τ-ϕ-τ-A, where ϕ stands for the pulse of optimized duration and A for the start of the data acquisition. Longitudinal relaxations were measured by saturation recovery (SR) with spin echo detection and by stimulated spin echos (SSE). The saturating sequence of the SR method is made of a series of pulses, separated by delays τ' such that $T_2<\tau'\ll T_1$. The full SSE sequence is ϕ-τ'-ϕ-τ-ϕ-τ'-A, where the longitudinal relaxation is reflected by the stimulated echo amplitude as a function of τ.

B. Nuclear magnetic interactions

In principle the La nucleus ($I=7/2$) is subject to transferred hyperfine and dipolar interactions with the electronic moments and to quadrupolar couplings to the electric field gradient.

Experimentally the characteristic quadrupolar spectrum (the powder singularities of the satellite frequencies) is never detected. However, the details of the multiexponential nuclear spin lattice relaxation indicate clearly that the quadrupolar frequency, ν_Q, is larger than the passband of the probe (say, 200 kHz), i.e., one cannot irradiate all the quadrupole-split transitions at once. This is confirmed by comparing the optimum excitation pulse in the 7 T NMR experiments with that of ^{2}H in deuterium dioxide ($^2\gamma\approx{}^{139}\gamma$): La requires shorter pulses by a factor 4–5, due to the larger effective γ of the $1/2\rightarrow -1/2$ transition. On the other hand, ν_Q must be just a few hundred kHz, because the compound is nearly cubic (for comparison $\nu_Q\approx 6$ MHz in La_2CuO_4, where the departure from cubic symmetry is large); therefore the NQR frequency is too low to be directly measured.

In these conditions the detected signal corresponds only to the central $1/2\rightarrow -1/2$ transition and the satellites must be severely inhomogeneously broadened by the presence of substitutions and vacancies. Therefore all the observed spectral features must result from magnetic interactions.

The La nucleus experiences a local field due to the electronic Mn moments given by

$$^{139}\mathbf{B}_i=\frac{2\pi}{^{139}\gamma}g\mu_B\sum_j \mathcal{C}_j\mathbf{S}_j+\mu_0\mathbf{H}+\mu_0\mathbf{H}_{dip}. \qquad (1)$$

Here $\mathbf{H}$ is the external field, which includes demagnetization terms when appropriate, $^{139}\gamma/2\pi=6.0145$ MHz/T the nuclear gyromagnetic ratio, and $\mathbf{H}_{dip}$ the dipolar sums over all Mn moments. The explicit sum on the right-hand side spans the eight nearest-neighbor moments $g\mu_B\mathbf{S}_j$, where $|\mathbf{S}_j|$ is proportional to the order parameter $S(T)$. The tensorial hyperfine coupling constants $\mathcal{C}_j$ reduce to scalar quanti-

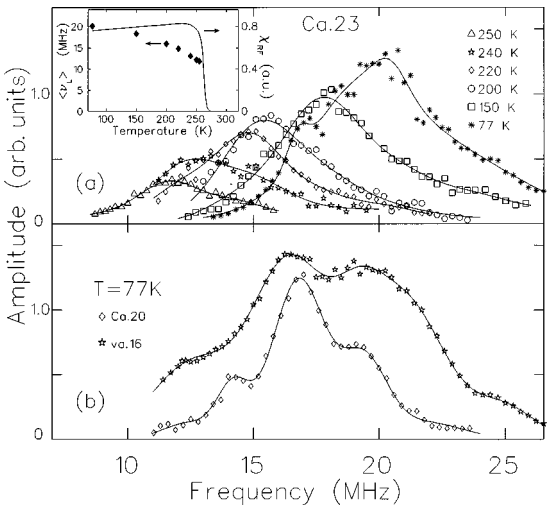

FIG. 1. (a) Zero-field spectra from sample Ca.23 at several temperatures below $T_c = 262$ K, indicating a spontaneous local field at the La nucleus; in the inset the diamonds show the average frequency as a function of temperature, while the solid line is the rf susceptibility. (b) Zero-field spectra from sample va.16 (stars) and sample Ca.20 (diamonds) at $T = 77$ K; the solid line is a multicomponent fit.

ties, because the largest contribution is from the overlap of the Mn orbitals with the on-site s-wave functions. We also neglect the distortion from the cubic symmetry and assume a single coupling constant $\mathcal{C}$ in the following. The dipolar fields cancel in a site of cubic symmetry and, when the symmetry departs from cubic, their powder spectrum has a vanishing first moment. Hence they may give rise to line broadening, but they do not contribute to the average resonance frequency.

Equation (1) predicts separate resonance frequencies for FM and AFM neighborhoods, because the sign of the transferred fields depends on the orientation of the neighbors; in particular, for a perfect AFM neighborhood the contributions to the transferred hyperfine field would cancel out exactly. This also means that antiferromagnetic spin fluctuations cannot be probed at the La site.

The equation also predicts distinct frequencies for defective magnetic neighborhoods, such as the substituted compounds,[27] where they give rise to well known patterns of satellite lines. The vacancy concentration itself is actually negligible in our samples, and we do not expect to see such satellites from vacancies, but similar patterns can arise from defects in the magnetic structure.

In the present work we exploit in part the characteristic rf enhancement of NMR in ferromagnetic compounds, which arises from the coupling of the electron moments to the rf field. The enhancement factor η is defined as the ratio of the internal rf field to the rf field applied in the sample coils; due to the hyperfine coupling a tilt of the electronic spin gives rise to a large field modulation on the nucleus. Such a mechanism takes place both inside a magnetic domain and in the domain walls; in the latter case the enhancement is generally much larger and it disappears upon saturation.

A final remark is due on the relaxation experiments. Magnetic spin lattice relaxation of a $I = 7/2$ nucleus with quadrupole splitting of the nuclear Zeeman levels is governed by

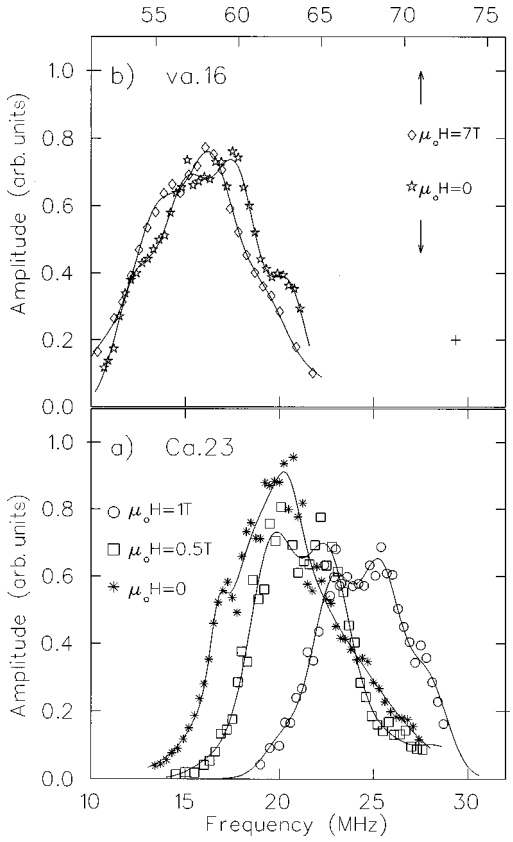

FIG. 2. (a) La NMR spectra at $T = 77$ K from sample Ca.23 in different applied magnetic fields. (b) La spectra at 0 and 7 T external field from sample va.16, below T_c ($T = 150$ K): notice the two distinct frequency scales.

master equations[28] which predict a multiexponential behavior. When only the central transition is irradiated one observes

$$M_{1/2\to -1/2}(t) = M_0\left(1 - \tfrac{4}{21}e^{-2Wt} - \tfrac{2}{11}e^{-12Wt} - \tfrac{20}{91}e^{-30Wt} - \tfrac{175}{429}e^{-56Wt}\right), \tag{2a}$$

$$M_{1/2\to -1/2}(t) = M_0\left(\tfrac{1}{84}e^{-2Wt} + \tfrac{3}{44}e^{-12Wt} + \tfrac{75}{364}e^{-30Wt} + \tfrac{1225}{1716}e^{-56Wt}\right), \tag{2b}$$

respectively, for SR and SSE experiments, which differ in the initial conditions. The transition probability $2W$ is identified with the rate $1/T_1$. With the same magnetic interactions the T_1-like contribution to the transverse relaxation (which in narrowing conditions dominates the single exponential envelope of the spin echo T_2 experiments) is given by $T_{2l}^{-1} = 16T_1^{-1}$, for $I = 7/2$, as it may be calculated following Ref. 29.

III. RESULTS

A. Zero-field and low-field experiments in FM samples

Zero-field NMR signals were observed in the 13–28 MHz band at 77 K in the three FM samples Ca.20, Ca.23, and va.16. The signal is very strong and it is characterized by a huge enhancement, typical of domain walls. The rf ampli-

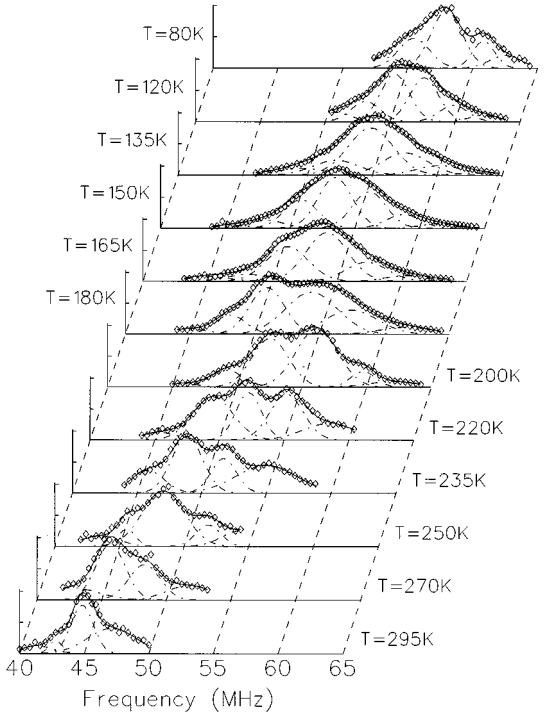

FIG. 3. NMR spectra from sample Ca.20 at different temperatures above and below $T_c = 180$ K. The solid lines are muticomponent best fits and the dashed-dotted lines are the individual components.

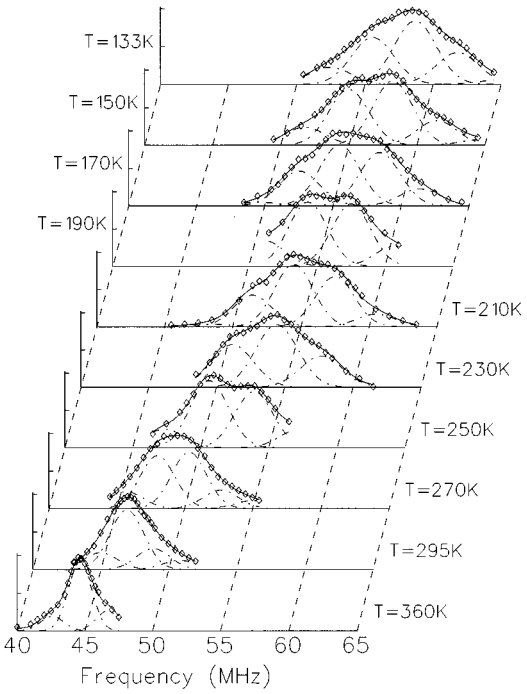

FIG. 4. NMR spectra from sample va.16 at 7 T at different temperatures above and below $T_c = 237$ K. The solid lines are multicomponent best fits and the dashed-dotted lines are the individual components.

tude employed is less than 10^{-3} of that required for nonmagnetic samples, yielding $\eta > 1000$.

The essential of the zero-field spectra is illustrated in Fig. 1. Panel (a) shows a series of spectra at different temperatures from sample Ca.23, the most extensively studied in this regime. The nonvanishing average resonance frequency indicates the presence of a spontaneous local field of hyperfine origin, according to Eq. (1). Its value, calculated from the first moment of the line, is shown in the figure inset as a function of temperature, superimposed to the rf macroscopic susceptibility $\chi_{\rm rf}$ (solid curve). The experimental values of the resonance frequency do not seem to vanish at T_c, where $\chi_{\rm rf}$ drops to zero. However, the NMR signal amplitude decreases approaching T_c, where it falls below the noise level. This fact has been pointed out previously,[21] and explained in terms of a critical temperature distribution in inhomogeneous samples. We shall argue in Sec. IV that chemical inhomogeneity is not the case.

The spectra from the other two samples, va.16 and Ca.20, shown in Fig. 1(b), are roughly similar. The average frequencies at 77 K are 18 and 17 MHz, respectively (cf. 20 MHz for Ca.23). They are all very broad, with FWHM of approximately 7–8 MHz, and clearly not single Gaussian. The best resolved of the underlying structure is that of Ca.20, where a main peak and two side shoulders can be clearly distinguished.

The domain wall origin of the signals of Fig. 1 is directly demonstrated by experiments in an external magnetic field. Sample saturation is achieved around $H_s = 0.5$ T: at this field the domain wall signal obtained at extremely low rf power disappears. A signal is recovered at the same frequency in the saturated sample upon amplifying the rf excitation by ca. 40 dB. The Ca.23 spectrum in $\mu_0 H = 0.5$ T is shown in Fig. 2(a), overlayed to the zero-field (ZF) one. The two spectra are centered at the same frequency of ≈ 20 MHz. The slightly larger width of the zero-field spectrum is fully justified by the more inhomogeneous domain wall environment.[30] The third spectrum in Fig. 2(a) corresponds to an external field of 1 T, above the average saturation value $H_s \approx 0.5$ T and it is shifted in frequency by $^{139}\gamma(H - H_s)$ without further distortions.

The same shift without broadening is nicely shown, in sample va.16, by Fig. 2(b), where the spectrum in 7 T at 150 K is overlayed onto the zero-field spectrum at the same temperature, with a frequency offset of 41.1 MHz. This offset corresponds to $\nu_L = {}^{139}\gamma/2\pi\mu_0(H - H_s)$ with an average saturation field $\mu_0 H_s = 0.17$ T. This close similarity of the two curves after the simple frequency shift indicates that both the hyperfine coupling *and* the magnetic susceptibility are isotropic, since anisotropies in either quantities would lead to a powder broadening of the 7 T spectrum.

B. FM samples in high magnetic field

We investigated samples Ca.20 and va.16 in 7 T, and in a large temperature range, $|T - T_c| \leq 100$ K. Spectra taken at different temperatures are shown in the multiple plots of Figs. 3 and 4, for Ca.20 and va.16, respectively. They are composed of several lines, as is particularly evident in the high temperature spectra of Ca.20 (Fig. 3). A good fit is achieved throughout the whole temperature range for both samples with a number of equally spaced Gaussian components of comparable widths. The solid curves in the figures are the best fits and the dashed lines show the individual components.

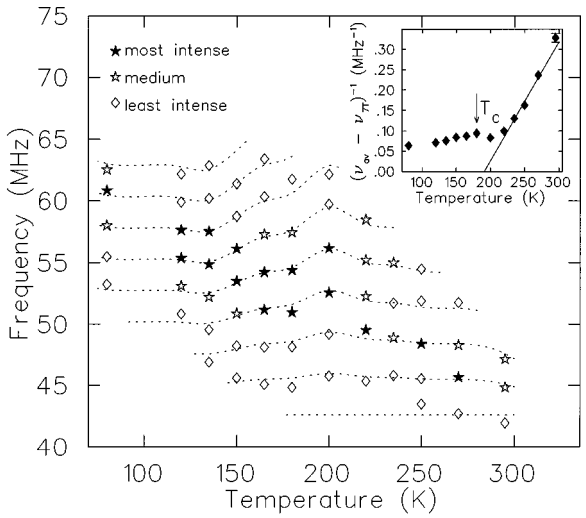

FIG. 5. Sample Ca.20: frequency of all peaks in the multicomponent best fit of Fig. 3, as a function of temperature. Different symbols identify the most intense, medium, and least intense components (dashed lines are a guide to the eye). Inset: inverse of the average frequency shift from the Larmor frequency as a function of temperature.

The center of all components is plotted as a function of temperature in Figs. 5 and 6, respectively, for Ca.20 and va.16. The most intense peaks are marked by filled stars. The dashed lines are meant just to guide the eye through the temperature evolution of each peak. For Ca.20 at intermediate temperatures this identification is more difficult and maybe not unique. However, the general trend is evident and very peculiar: for both samples the center of each Gaussian peak is very weakly temperature dependent, whereas the spectral weight progressively shifts from one peak to the adjacent higher frequency ones as the temperature is lowered.

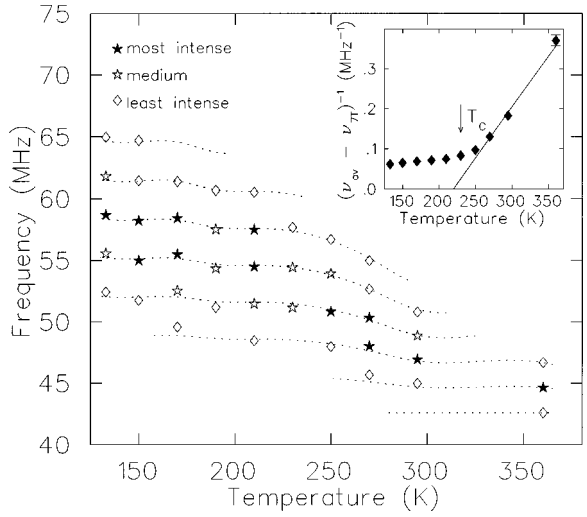

FIG. 6. Sample va.16: frequency of all peaks in the multicomponent best fit of Fig. 4, as a function of temperature. Different symbols identify the most intense, medium, and least intense components (dashed lines are a guide to the eye). Inset: inverse of the average frequency shift from the Larmor frequency as a function of temperature.

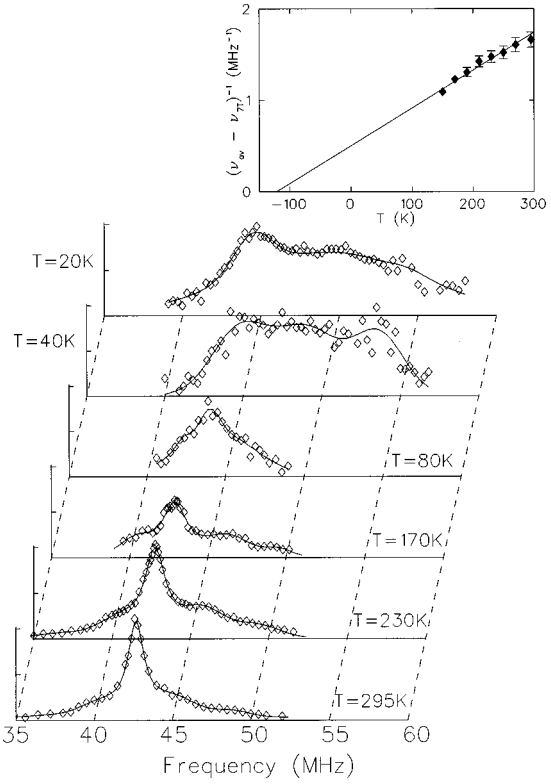

FIG. 7. NMR spectra from sample va.00 at 7 T at a few different temperatures. The solid lines are multicomponent best fits. Inset: inverse of the frequency shift for the central component vs temperature, and Curie-Weiss law (solid line) extrapolating to negative temperatures.

The average frequency shift, which may be obtained from the first moment of each spectrum, ν_{av}, varies smoothly with temperature. According to Eq. (1), $\nu_{av}-\nu_L$ measures an average of the order parameter (note that in 7 T it does not vanish above T_c). A plot of its inverse versus temperature is given in the insets of Figs. 5 and 6. The points at $T \gg T_c$ follow a Curie-Weiss law $(\nu_{av}-\nu_L)/\nu_{hf} = (ngS\mu_B)^{-1}CH/(T-\theta)$, where ν_{hf} is the hyperfine frequency, with a large value of C of order 0.24 K (cf. $4\mu_B$ yield 0.083 K), similar to that obtained from macroscopic susceptibility.[25] The values of the intercept are $\theta = 220 \pm 10$ K (va.16) and 190 ± 15 K (Ca.20) in agreement with those of Table I.

C. AFM $LaMnO_3$ in high magnetic field

A set of zero-field La spectra from the nominally AFM sample va.00 have already been published,[20] demonstrating the presence of a net FM hyperfine on a sizable fraction of La nuclei below 80 K. La NMR spectra in 7 T were recorded on the same sample over a wide temperature interval, from the paramagnetic state at room temperature down to 20 K, well within the magnetically ordered state.

At room temperature the spectrum (Fig. 7) consists of a sharp, nearly Lorentzian peak ($\Delta\nu$ FWHM$\simeq$1 MHz) centered at 42.6 MHz, and a very broad background. The peak displays a paramagnetic shift, $\Delta\nu = \nu - \nu_L = 580$ kHz, which increases smoothly with decreasing temperature according to a Curie-Weiss law $\Delta\nu/\nu_{hf} = ngS\mu_B CH/(T+\theta)$, with nega-

tive intercept, as expected of an antiferromagnet. The best fit for the intercept (inset of Fig. 7) is $\theta = 150 \pm 50$ K, compatible with the T_N values reported by neutron diffraction,[10] and the Curie-Weiss constant is $C = 0.17$ K, comparable to the value found for the FM lines.

Two lobes can be clearly distinguished in the broad background of the paramagnetic spectra, at approximately ± 3 MHz on either sides of the central peak. Their origin is magnetic and must be reconciled with Eq. (1). Below 210 K the NMR signal amplitude decreases and it is completely lost at $T \approx 130$ K, due to fast inhomogeneous transverse relaxation rates. Comparison between the $T = 230$ K and $T = 170$ K spectra of Fig. 7 shows that the reduction is more severe on the central peak than on the broad component. Similar results are obtained from sample va.11 throughout this temperature range.

No signal is detected between 130 K and 90 K, an interval encompassing the transition temperature of Table I. A broad NMR signal is recovered at $T \approx 90$ K, with no sign of a sharp peak close to ν_L (Fig. 7, top). The width of the spectrum and its average shift increase at low temperatures (FWHM$\approx$5 MHz, $\nu_{av} \approx 44.5$ MHz at 80 K vs FWHM$\approx$10 MHz, $\nu_{av} \approx 49$ MHz at 40 K). The signal amplitude grows decreasing the temperature more than predicted by the nuclear susceptibility, $\chi_n \propto 1/k_B T$, indicating an increase of the fraction of nuclei contributing to this signal.

The positive average shift below 90 K, $\nu_{av} - \nu_L$, coincides with the average hyperfine frequency detected in zero external field. Since the sum over the hyperfine terms of Eq. (1) would cancel out for AFM ordering we assign the signal to a ferromagnetic environment. We further note that the spectra are similar to those of Figs. 7, 5, and 6: for instance, the 20 and 40 K spectra of the present sample show a trace of the multicomponent pattern displayed by Ca.20 and va.16.

The nuclei belonging to the AFM domains, identified in the paramagnetic range, should give rise to an NMR signal close to ν_L, which is not detected, even in the 20 K spectrum, probably owing to fast T_2 relaxations (this is the reason for the absence of a ^{55}Mn AFM signal above 4.2 K in this sample).

D. Relaxations

The rates of the spin lattice relaxation (SLR) and of the spin spin relaxation (SSR) were investigated in all samples. They display a remarkably different behavior in the AFM samples (va.00, va.11), with respect to the FM samples (Ca.20, va.16, and Ca.23). We shall report on three representative sets of data: relaxations in samples va.00 and va.16 in 7 T as a function of temperature, and in sample Ca.23 below T_c as a function of the applied field, between 0 and 1 T.

Let us start from the fully FM sample va.16, whose relaxation rates are summarized in Fig. 8. Panel (a) shows the dependence of the nuclear magnetization upon the delay time in the pulse sequence, in the two distinct spin lattice relaxation experiments performed (SR and SSE; cf. Sec. II B). Both agree very well with the multiexponential behavior predicted by Eqs. 2(a) and 2(b), represented by the two solid curves in the figure, which yield fully consistent best fit values of the rate $2W$. SSR raw data at two representative temperatures are shown in panel (b). Above 250 K (e.g., 295 K

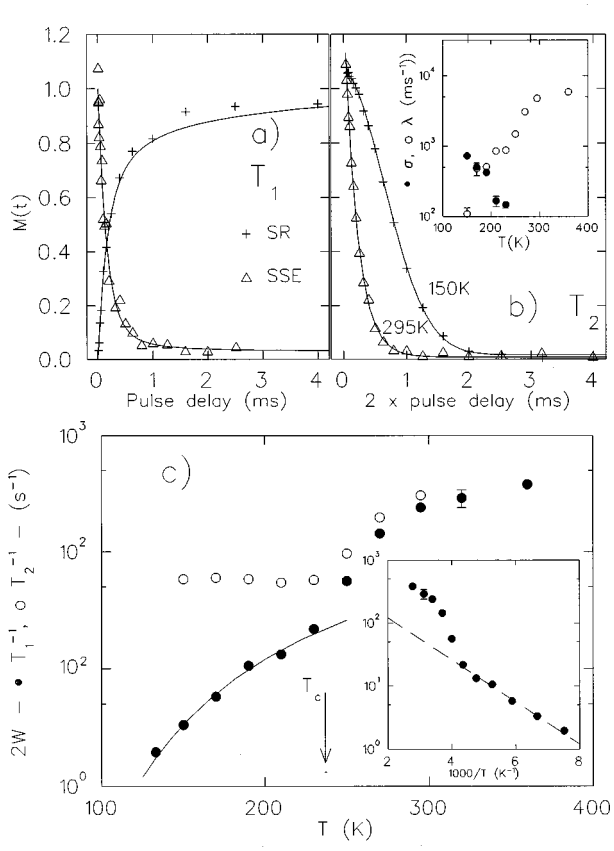

FIG. 8. Sample va.16: (a) Spin lattice relaxation vs time by saturation recovery (SR) and stimulated spin echo (SSE) at 295 K; the solid curves are best fits to Eq. (2). (b) Spin spin relaxation vs time. The solid curves are fit to $e^{-\lambda t} e^{-\sigma^2 t^2/2}$ and the temperature dependence of σ and λ is plotted in the inset. (c) $2W$ from SLR and SSR rates vs temperature (SLR in the inset on a log scale). The solid curve (the dashed line in the inset) is the Arrhenius best fit (see text).

in the figure) the data follow a single exponential behavior, with an SSR rate $T_2^{-1} = 16 T_1^{-1}$, as predicted by the relevant expression just below Eq. 2(b). Below 250 K the relaxation curve acquires a Gaussian component and eventually becomes fully Gaussian around 150 K [see the second curve in panel (b)]. The fitted Gaussian and Lorentzian rates are shown in the inset of Fig. 8(b) as a function of temperature. The Gaussian relaxation at 150 K ($\sigma = 10^3$ s^{-1}) corresponds to a static homonuclear homogeneous width.

The temperature dependence of $2W$ from SLR and of the corresponding quantity from the SSR curves are shown in Fig. 8(c). For the sake of simplicity we plot the same Lorentzian fit parameter also for the SSR rate below T_c (arrow in the plot), in place of the more correct deconvolution of Fig. 8(b), inset, whose Lorentzian component acquires a very large error in this range. The plateau in the SSR below T_c indicates that a static contribution dominates. Above T_c the SSR and the SLR rates become proportional, both rapidly increasing with temperature. This fact implies that the SLR rate and the dominant T_1-like component of the SSR rate are due to fast (magnetic) fluctuations, in the narrowing regime. The increase with temperature must be due to an increase in the instantaneous intensity of the relevant fluctuating fields, i.e., in the density of fast fluctuations. The behavior of

sample Ca.23 was less thoroughly studied, but is fully consistent with that of sample va.16.

Our data do not show signs of a ferromagnetic critical divergence of the relaxation rates, which is, however, not surprising in a soft ferromagnet, considering that a large magnetic field is applied. Below T_c the SLR rate still decreases with T, following an Arrhenius behavior $2W \propto \exp(-T_a/T)$, with $T_a = 700(50)$ K, as the solid line in the inset of panel (c) demonstrates. The solid curve in the main panel, which is the same Arrhenius function, shows that there is a change of slope in the SLR rate at T_c. Comparing the behavior below and above the transition, the Arrhenius fit indicates that for $T > T_c$ there is an additional contribution to the relaxation rates, which vanishes exactly at T_c. This suggests that not only a ferromagnetic critical divergence is absent, but furthermore an *antidivergence* appears in its place. We shall come back to this point, which may be the sign of the development of a peak in the spin-spin correlation function at the antiferromagnetic wave vector.

A very different picture emerges from the nominally AFM sample va.00. Here too the SLR is multiexponential. The values of $2W_1$ extracted from the SLR rate in an applied magnetic field of 7 T are shown in Fig. 9 as a function of temperature, well above the transition ($T_c = 115$ K). The room temperature values are similar to those of sample va.16. A second value, $2W_2$, is also plotted; according to the discussion below Eq. 2(b) it represents 1/16 of the fitted single exponential SSR rate, which agrees remarkably well with the $2W_1$ values above 200 K. This fact implies that the relaxation process at high temperatures is in the narrowing regime of fast fluctuations. The value of $2W_2$, however, increases drastically for decreasing temperatures, eventually killing the signal, while the SLR rate develops a maximum around 190 K and it decreases below that temperature. This implies a crossover towards a static regime.

A satisfactory fit is given by the solid line which implements a crude dynamical model:[31] the electronic moments produce an instantaneous local field (by assumption the value measured in the ordered phase, corresponding to a hyperfine frequency of 20 MHz), with a thermally activated correlation time $\tau(T) = \tau_0 \exp(T_a/T)$, yielding the following rates

$$2W_1 = \frac{2\omega_0^2 \tau}{1+\omega_e^2 \tau^2}; \quad 2W_2 = \frac{\omega_0^2 \tau}{1+\omega_e^2 \tau^2} + \omega_0^2 \tau. \tag{3}$$

The best fit values are $T_a = 700(20)$ K for the activation temperature, $\tau_0 = 1.4(1)10^{-14}$ s for the preexponential correlation time, and $\omega_e = 1.7\ 10^{12}\ \mathrm{s}^{-1}$ for the electron frequency (of the same order of magnitude as $g\gamma_e\mu_0 H$). This term describes an interaction with an electronic magnetic field mediated by an isotropic hyperfine interaction $\mathcal{C}\mathbf{I}\cdot\mathbf{S}$. It shall be commented upon in the next section.

Finally, we measured the low temperature SSR and SLR rates in zero field in the FM sample Ca.23. Both are nearly independent of frequency across the broad spectrum and the time dependence of the nonequilibrium nuclear magnetization is well described by a stretched exponential law $\delta M_{\perp,\parallel} \propto \exp[-(t/T_{1,2})^{\beta}]$, with best-fit parameters at $T = 77$ K $1/T_1 = 330\ \mathrm{s}^{-1}$, $\beta \approx 0.5$ for the SLR, and $1/T_2 = 2500\ \mathrm{s}^{-1}$, $\beta \approx 0.6$ for the SSR.

The stretched exponential relaxation is characteristic of domain wall signals. The dominant mechanism of relaxation is due to domain wall fluctuations,[32] which may themselves be viewed as enhanced fluctuating fields at the nucleus. However, the enhancement η is very inhomogeneous across a Bloch wall; this leads to a distribution of relaxation rates, resulting in the stretched exponential behavior.[33,34]

The SSR single exponential relaxation law is restored by fully saturating the sample magnetization in an external field of 1 T at 77.3 K and the SSR rate becomes smaller by a factor 3. The longitudinal relaxation function becomes compatible with that predicted by the master equations, as in the case of va.16 at 7 T, although a strong dependence of the SSR rate on the irradiation bandwidth indicates a relevant spin diffusion contribution to the observed relaxation, which is reduced at higher fields.[35] However, the most prominent feature is the decrease of the SLR rate by two orders of magnitude, which indicates that the longitudinal relaxation in the saturated sample probes the bulk spin fluctuations rather than the domain wall motion. Both SSR and SLR rates in the saturated sample are close to the corresponding ones in va.16 at 7 T, so that the last conclusion may be safely extended to all fully FM samples.

IV. DISCUSSION

The La zero-field spectra indicate the presence of a full low temperature hyperfine field on La of the order of 0.5 T from each of its eight FM Mn neighbors. Considering $3.77 < g\langle S(0)\rangle \leqslant 4\mu_B$ in our samples (spin-only g factor), this corresponds to a coupling constant $\mathcal{C} \approx 0.13T/\mu_B$. The detection of nuclei experiencing such a hyperfine field in all samples, including va.00,[20] confirms that FM domains are present in all compositions.

The hyperfine field is also identified in the La NMR spectra of all $LaMnO_3$ Ca-doped samples. They consist of patterns of peaks, each corresponding to the hyperfine field transferred from a number of ferromagnetically ordered Mn nearest-neighbor ions, collinear to the external field. The La hyperfine constant $\mathcal{C}$ is positive, as expected, since the NMR line shifts to higher frequency in an applied external field. The low saturation values seen in all FM samples and the absence of powder broadening in all high-field experiments confirms the Mn NMR findings of very soft magnetic properties and isotropic hyperfine couplings. The peak pattern is more or less pronounced, but it is common to both AFM and FM samples.

We concentrate first on the 7 T spectra of FM samples where the peaks are sharpest. Their positions are equally spaced (by an amount corresponding to the hyperfine field due to one nearest-neighbor Mn) and nearly independent of temperature; the spectral weight is transferred from lower to higher frequency peaks as the temperature is lowered. Thus each of the eight dashed lines in Fig. 6 (the pattern in Fig. 5 is similar, but more complex) corresponds to La nuclei resonating in a hyperfine field transferred, according to Eq. (1), from 0,1,...,7 neighboring Mn ions (peak 8 is absent, down to 77 K). Hence the La peaks *count* the number of FM nearest-neighbor (NN) Mn moments collinear to the external field. An apparently similar interpretation, based on a defective spin neighborhood of the resonating nucleus, holds for the

^{55}Mn NMR spectra of $La(Ni_{1-x}Mg_x)_{0.5}Mn_{0.5}O_3$ at 4.2 K,[27] where random substitution of Ni with nonmagnetic Mg gives rise to equally spaced satellite lines. This is, however, a very surprising feature in our system, since here the spin defects cannot be due to chemical composition, because the percentage of vacant Mn sites is negligible, while the experimental defect fraction, close to T_c, is huge. A conservative estimate of the vacant Mn fraction is, for instance, to assume that all the Mn^{4+} excess charge is due to vacancies—clearly a gross overestimate for the Ca-doped samples. In va.16, for instance, 0.16 Mn^{4+} would correspond to 0.063 vacancies per formula unit: this leads to temperature independent fractions of La with zero, one, and two NN vacant Mn sites (peaks 8, 7, and 6), respectively, equal to 0.65, 0.29, and 0.06. Furthermore, the experimental defect fraction changes dramatically with temperature, which means that it is controlled by thermal excitations rather than by stoichiometry.

The occurrence of peaks with an odd number of hyperfine contributions is also noteworthy, since configurations consisting just of spins parallel and antiparallel to the field would only produce even order peaks, on the basis of Eq. (1). This consideration allows us to rule out a few simple options: (i) A perfect FM site, where eight equal NN moments would be all parallel to the external field, yielding a single high resonance frequency, $\nu-\nu_L=8g\mu_B\mathcal{C}S(T)$; (ii) a perfect AFM site, where the hyperfine terms would cancel out (furthermore the eight equal NN moments would be perpendicular to the external field, since $\chi_\perp^{AFM}>\chi_\parallel^{AFM}$); (iii) a FM configuration with NN *localized* FM Mn^{4+} ions, since $n=0,\ldots,8$ Mn^{4+} moments ($3\mu_B$ each) and $8-n$ Mn^{3+} moments ($4\mu_B$ each) yield a resonance frequency pattern removed from the Larmor frequency, $\nu-\nu_L\approx(8-n/4)g\mu_B\mathcal{C}S(T)$. We conclude that the experimental patterns are due to immobile ''defects'' in the FM structure (either fluctuating moments or moments perpendicular to the applied field). They also produce a net dipolar field on La, whose powder average is responsible for the observed width of the peaks (ca. 3 MHz).

This brings up another question: are the defects randomly placed, or do they display short range order (SRO)? An indirect support for SRO comes from the Gaussian SSR observed in va.16 at 150 K (Fig. 8): the experimental value of $\approx10^3$ s^{-1} is reduced only by a factor 3.5 with respect to the calculated homonuclear dipolar second moment. Actually, in view of the ca. 3 MHz inhomogeneous broadening of the peaks, one expects that two spins whose resonance frequencies are separated by more than $(2\pi T_2)^{-1}$ ought to act as *unlike spins* and should not contribute to each other's relaxation, due to the refocusing action of the spin echo. This would yield a very much larger reduction (by a factor $3\pi10^6/10^3$) of the T_2^{-1} measured in a spin echo experiment, and an exponential decay—as from dilute impurities. If, however, the defects belong to a SRO superstructure they distinguish only a few inequivalent La sites, and all equivalent La nuclei contribute to their own relaxation. The reduction in this case is proportional to the square root of the number of inequivalent sites, which is a small factor, compatible with 3.5.

An alternative view is that the observed signal derives from densely packed FM clusters, which may result in a large fraction of La nuclei in the boundary regions. This would lead to a defect distribution intermediate between the SRO and the homogeneous random displacement. We have invoked similar self-segregated FM microdomains to explain the coexistence of AFM and FM Mn signals and their cross coupling.[20] These clusters may be connected with the detailed structure of the Jahn-Teller polarons which are responsible for the large isotope effects on T_c and on the EPR relaxation.[16,17]

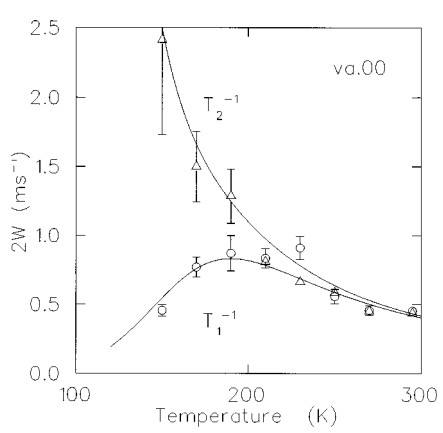

FIG. 9. NMR relaxation rates $2W_1$ and $2W_2$ (from SLR and SSR, respectively) as a function of temperature, from sample va.00 at $\mu_0H=7$ T. The solid line is a fit to Eq. (3).

Only single crystal NMR data (or small angle scattering) could clarify this structural issue. For the time being we shall focus on the defect distribution and compare our results with the simple binomial distribution, which implies a neglect of correlations. If z is a temperature—and maybe also field—dependent fraction of FM moments ($1-z$ is the defect fraction), the probability p_n of La having n such nearest neighbor and the corresponding resonance frequency ν_n [see Eq. (1)] are

$$\nu_n(T)=\nu_L+ng\mu_B\mathcal{C}S(T), \quad p_n=C(8,n)z^n(1-z)^{8-n}, \tag{4}$$

where $C(8,n)=8!/n!(8-n)!$.

We compared this distribution with the 7 T results on Ca.20, where the multipeak pattern is more evident, fitting the weights and frequencies of the spectral components plotted in Fig. 3. Least square deviations are obtained by varying z and the average frequency step, $g\mu_B\mathcal{C}S(T)$, of Eq. (4) at each temperature. The behavior of the two parameters is shown in the main panel of Fig. 9; a typical fit of this kind is shown in the inset, where the weights of the spectral components (open circles) are slightly more peaked than the fitted binomial distribution (solid line). A similar reasonable agreement is obtained at all temperatures.

It must be noted that the existence of a binomial distribution does not solve the structural issue: the binomial may arise either from a homogeneous random distribution of defects [where $1-z(T)$ is the site probability of the defect] or

from a thermal distribution of different SRO structures [where $1-z(T)$ is the average defect probability over all the structures present at temperature T].

While the fraction z increases almost continuously upon lowering the temperature (hence the defect fraction $1-z$ decreases with T) the average frequency step, $g\mu_B\langle S\rangle\mathcal{C}$, does not follow a simple magnetization curve. It is rather flat above $T_c=180$ K, and it shows a *decrease* below this temperature, which could either be due to structural changes at T_c (through $\mathcal{C}$) or to a reentrant behavior of $S(T)$. Similar fits for sample va.16 do not show the reentrant behavior. For both va.16 and Ca.20 the order parameter is very large above T_c, much more than predicted by mean-field theory for the Mn^{3+} moment in a field of 7 T. This is an indication of larger clusters of spins acting as single entities, consistent with magnetization and recent small angle neutron scattering results.[15] We recall that also the zero-field measurements of Fig. 1 (inset) on Ca.23 show an unconventional dependence of the order parameter on temperature very close to T_c.

As the spectrum changes continuously, with no qualitative differences across the transition, a similar rather smooth variation is displayed by the relaxations, with no critical divergence in the SLR and SSR rates, but rather a reduction of the rate on approaching T_c. This reduction actually looks like an antidivergence, if one subtracts the low temperature Arrhenius behavior from the data of Fig. 8 [see, e.g., the excess relaxation above T_c in Fig. 8(c)]. A critical relaxation peak was indeed observed by zero-field μSR (Refs. 36, 37), but its absence here, as well as the continuous spectral variation across T_c, could just be due to the large (7 T) applied magnetic field of the NMR experiment. As a matter of fact, in principle there is no critical point for a ferromagnet in a magnetic field, and in practice critical FM fluctuations in these soft materials are quenched by rather small fields.[38] Still, the presence of an antidivergence at T_c remains a surprising feature.

For both probes, La and muon, the SLR is $T_1^{-1}\propto\Sigma_q f_{La,\mu}(q)\chi''(q,\omega_L)/\omega_L$, where χ'' is the dynamic spin susceptibility, ω_L the Larmor frequency, and $f_{La,\mu}(q)$ a form factor reflecting the symmetry of the probe's position with respect to the fluctuating moments. The muon and residual high-field La relaxations can be reconciled only if one assumes that a component of χ'' is developing a peak at the antiferromagnetic wave vector q_{AFM}. In this case the zero-field muon relaxation is dominated by the ferromagnetic modes, which are quenched in the high-field NMR experiment. However, since the La site is symmetric between the two AFM sublattices, one has $f_{\mathrm{La}}(q_{AFM})=0$ and thus, when the fluctuation spectral weight of the AFM component is shifted from $q=0$ towards q_{AFM}, the La nuclear relaxation rate displays an antidivergence.

The issue is then why a macroscopically FM transition should be accompanied by an AFM component of χ''. We are thus led to suggest the diffusion of an AFM correlated localized mode, which freezes out at the onset of FM order, as the source of fluctuation probed by La close to T_c. Actually both the muon and the La rates vary on a rather broad temperature interval and hint at a diffusive, rather than a critical nature of the fluctuations. Also the peculiar shape of the muon relaxation function (stretched exponential) and the relatively small peak observed for the rate ($\Lambda_{\max}=0.4\ \mu s^{-1}$) are uncommon for standard FM critical fluctuations, and may partly reflect this composite nature of the fluctuations.

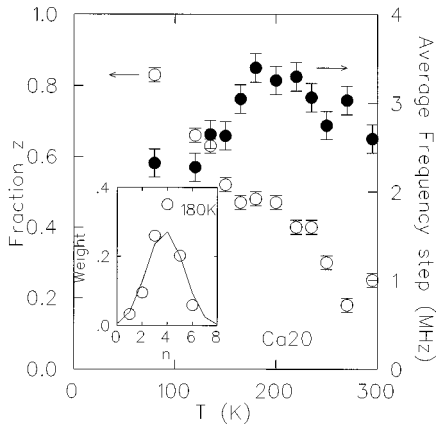

FIG. 10. Fraction z (open symbol) and frequency step $g\mu_B S(T)\mathcal{C}$ (filled symbol), obtained from a fit of the Ca.20 spectra to the binomial distribution of Eq. (4) (see text). The inset shows a typical fit (solid line) of the spectral weights (circles) from the multicomponent spectra of Fig. 3, as a function of the number $n=0,\ldots,8$ of nearest-neighbor FM ordered moments.

The diffusive character of excitations may be the result of spin dynamics dictated by a Hund-rule exchange energy $J\gg k_B T_c$, as is predicted by polaronic models, where T_c is proportional to the polaron effective bandwidth W_{eff}.[16–18] In this respect also the low temperature Arrhenius behavior of the La SLR [Fig. 8(c)] is significant, as it corresponds to a fairly large energy scale ($T_a=700$ K). In a conventional magnetic material it would suggest a gap to magnetic excitations, in contrast with the soft magnetic properties of these materials. In the context of magnetic polarons, however, the condition $T_c\propto W\ll J/k_B$ would correctly predict much reduced nuclear relaxations for $T<T_c\ll J/k_B$.

Let us now concentrate on static AFM-ordered domains, which were expected only at the low x end of the phase diagram, but were identified by Mn NMR in all these samples, including the FM ones.[20] Unfortunately, they cannot be directly detected by zero-field La NMR because there is no net AFM hyperfine field on La. Thus the only direct signature of AFM domains in the present experiment is the inverse frequency shift of Fig. 7 (inset), which extrapolates to negative temperatures. This shift belongs to the narrow component of the 7 T NMR spectra above T_c, which is prominent only in samples with $0\leqslant x\lesssim 0.11$ and is therefore identified with the AFM domain contribution above the transition temperature. The relaxation rates of this line (Fig. 9) are very large and display a totally different behavior with respect to the FM signal discussed above.

Here a slowing down of the local field fluctuations is evident: while $2W_1$ and $2W_2$ coincide and decrease at high temperature, indicating the onset of a motional narrowing regime, below $T\approx 190$ K the behavior of the two rates is typical of a crossover to a static regime. Note that the peak in $2W_1$ versus temperature is *not* a divergence, but rather the mark of this crossover, which is determined, on the time scale of the NMR measurement, by the condition $\omega_e\approx 1/\tau(T)$. This is confirmed by the fit to Eq. (3), which is quite satisfactory. In particular, fixing the magnitude of the instantaneous local field at La to the static low temperature

value yields an electron energy scale $\hbar\omega_e$ of the right order of magnitude, the correlation between these two parameters in the model of Eq. (3) being too high to allow them to be both varied. The value of the activation temperature, $T_a \approx 700$ K, is similar to that obtained in the FM sample va.16, below T_c.

Surprisingly, therefore, the temperature dependence of the fluctuations responsible for the nuclear relaxation in va.00 displays a diffusive, rather than critical, character. Furthermore, the correlation within the diffusing excitation must be of FM nature, since by symmetry AFM-type correlations do not produce a net field on La. We are led to conclude that we are detecting the diffusion of a localized FM excitation over a region which will develop AFM order upon cooling below the transition. Recent μSR results on materials at this end of the phase diagram show longitudinal relaxations fully consistent with this picture.[37]

Summarizing, the nuclear relaxation in FM and AFM samples are complementary in that they can be described respectively in terms of localized AFM correlations diffusing across a FM background, for va.16, and of localized FM correlations diffusing across an AFM background, for va.00. It seems that a *homogeneous* picture, even if based on double exchange plus electron-phonon couplings and Jahn-Teller distortions is not complete, and that electronic phase separation connected with *small* magnetic JT polarons must take place as well.

V. Conclusions

Our results confirm the striking Mn NMR evidence[20] for FM microdomains in the end member $LaMnO_3$ itself, with the direct detection of zero-field resonance frequencies due to a net hyperfine field, which would be absent in an AFM surrounding. The corresponding NMR spectra indicate that the hyperfine coupling is isotropic and its positive value is slightly in excess of 0.1 T/μ_B.

The NMR shifts in the paramagnetic phase scale always with Curie-Weiss laws. This behavior distinguishes nuclei in FM neighborhood, present in all the samples, from those in AFM neighborhood (only present in va.00 and va.11), characterized by a negative zero intercept of the inverse susceptibility. The phase diagram described by these transition temperatures coincides with that obtained from the rf susceptibility data of Table I.

A very peculiar magnetic structure is revealed by the NMR spectra in the FM samples, with a high abundance of magnetic defects, signaling inhomogeneous spin arrangements, either due to short range ordered structures or to a coexistence of FM and AFM clusters.

Relaxations distinguish the static FM environment from the AFM one, since the former witnesses the diffusion of AFM cluster, while the latter experiences time dependent FM correlations.

In conclusion, La NMR of manganites in the $0 < x < 0.23$ range support the Mn NMR interpretation based on intrinsically inhomogeneous magnetic order on a microscopic scale, which develops at low temperature into the intimate mixture of FM and AFM correlated domains also observed by Mn NMR.

ACKNOWLEDGMENTS

The authors are very glad to acknowledge very stimulating discussions and useful criticism from C. Bucci and M.W. Pieper. The samples, their chemical characterization, and illuminating material science information were provided by F. Licci.

[1] G. H. Jonker and J. H. Van Santen, Physica (Utrecht) **16**, 336 (1950).
[2] S. Jin, T. H. Tiefel, M. McCormack, R. A. Fastnacht, R. Ramesh, and L. H. Chen, Science **264**, 413 (1994).
[3] S. Jin, M. McCormack, T. H. Tiefel, and R. Ramesh, J. Appl. Phys. **76**, 6929 (1994).
[4] R. von Helmolt, J. Wecker, K. Samwer, L. Haupt, and K. Bärner, J. Appl. Phys. **76**, 6925 (1994).
[5] C. Zener, Phys. Rev. **82**, 403 (1951).
[6] J. B. Goodenough, Phys. Rev. **100**, 565 (1955).
[7] P. W. Anderson and H. Hasegawa, Phys. Rev. **100**, 675 (1955).
[8] P. G. de Gennes, Phys. Rev. **118**, 141 (1960).
[9] K. Kubo and N. Ohata, J. Phys. Soc. Jpn. **33**, 21 (1972).
[10] E. O. Wollan and W. C. Koehler, Phys. Rev. **100**, 545 (1955).
[11] H. Kawano, R. Kajimoto, M. Kubota, and H. Yoshizawa, Phys. Rev. B **53**, 2202 (1996).
[12] A. J. Millis, P. B. Littlewood, and B. I. Shraiman, Phys. Rev. Lett. **74**, 5144 (1995).
[13] A. J. Millis, B. I. Shraiman, and R. Mueller, Phys. Rev. Lett. **77**, 175 (1996).
[14] A. J. Millis, R. Mueller, and B. I. Shraiman, Phys. Rev. B **54**, 5389 (1996); **54**, 5405 (1996).
[15] J. M. De Teresa, M. R. Ibarra, P. A. Algarabel, C. Ritter, C. Marquina, J. Blasco, J. Garcia, A. del Moral, and Z. Arnold, Nature (London) **386**, 256 (1997).
[16] Guo-meng Zhao, K. Coder, H. Keller, and K. A. Müller, Nature (London) **381**, 676 (1996).
[17] A. Shengelaya, Guo-meng Zhao, H. Keller, and K. A. Müller, Phys. Rev. Lett. **77**, 5296 (1996).
[18] K. H. Hock, H. Nickisch, and H. Thomas, Helv. Phys. Acta **50**, 235 (1983).
[19] E. L. Nagaev, Phys. Status Solidi B **186**, 9 (1994); JETP Lett. **6**, 484 (1967); Sov. Phys. JETP **27**, 122 (1968).
[20] G. Allodi, R. De Renzi, G. Guidi, F. Licci, and M. Pieper, Phys. Rev. B **56**, 6036 (1997).
[21] M. K. Gubkin, A. V. Zalesskii, V. G. Krivenko, T. M. Perekalina, K. A. Khimich, and V. A. Chubarenko, JETP Lett. **60**, 56 (1994).
[22] J. A. M. Roosmalen, E. H. P. Cordfunke, and R. B. Helmolt, J. Solid State Chem. **110**, 100 (1994).
[23] F. Licci, G. Turilli, and P. Ferro, J. Magn. Magn. Mater. **164**, L268 (1996).
[24] P. G. Radaelli, D. E. Cox, M. Marezio, S-W. Cheong, P. E. Schiffer, and A. P. Ramirez, Phys. Rev. Lett. **75**, 4488 (1995); R. Mahendiran *et al.*, Phys. Rev. **53**, 3348 (1996).
[25] G. Allodi and M. Solzi (unpublished).

[26] R. Mahesh, R. Mahendiran, A. K. Raychaudhun, and C. N. R. Rao, J. Solid State Chem. **120**, 204 (1996).
[27] M. Sonobe and K. Asai, J. Phys. Soc. Jpn. **61**, 4193 (1992).
[28] M. I. Gordon and M. J. R. Hoch, J. Phys. C **11**, 783 (1978).
[29] R. R. Ernst, G. Bodenhausen, and A. Wokaun, *Principles of Nuclear Magnetic Resonance in One and Two Dimensions* (Oxford Univ. Press, Oxford, 1987), p. 55.
[30] P. C. Riedi, Hyperfine Interact. **49**, 335 (1989).
[31] N. Bloembergen, E. M. Purcell, and R. V. Pound, Phys. Rev. **73**, 679 (1948).
[32] M. Weger, Phys. Rev. **128**, 1505 (1962).
[33] J. Barak, I. Siegelstein, A. Gabai, and N. Kaplan, Phys. Rev. B **8**, 5282 (1973).
[34] M. W. Pieper, J. Kötzler, and K. Nehrke, Phys. Rev. B **47**, 11 962 (1993).
[35] W. W. Simmons, W. J. O'Sullivan, and W. A. Robinson, Phys. Rev. **127**, 1168 (1962).
[36] R. H. Heffner *et al.*, Phys. Rev. Lett. **77**, 1869 (1996).
[37] G. Allodi, L. Cristofolini, and R. De Renzi (unpublished).
[38] R. H. Heffner *et al.*, Physica B **230-232**, 759 (1997).